Science of the Total Environment 756 (2021) 143830

Contents lists available at ScienceDirect

Science of the Total Environment

journal homepage: www.elsevier.com/locate/scitotenv

Long-term spatiotemporal variability in high Andean wetlands in northern Chile

Alberto de la Fuente [a,*], Carolina Meruane [a,b], Francisco Suárez [c,d,e]

[a] Departamento de Ingeniería Civil, Universidad de Chile, Santiago, Chile
[b] Modelación Ambiental SpA, Chile
[c] Departamento de Ingeniería Hidráulica y Ambiental, Pontificia Universidad Católica de Chile, Santiago, Chile
[d] Centro de Desarrollo Urbano Sustentable (CEDEUS), Santiago, Chile
[e] Centro de Excelencia en Geotermia de los Andes (CEGA), Santiago, Chile

HIGHLIGHTS

- Size of wetlands is determined by the balance of groundwater and evaporation.
- Wetlands grow and shrink in response to seasonal changes in evaporation.
- Groundwater recharge is infrequent with a period of recurrence of 20 to 30 years.
- Wetlands' size gradually decreases as groundwater reservoir empties between wet years.
- The Tropic of Capricorn is a natural boundary for classifying high Andean wetlands.

GRAPHICAL ABSTRACT

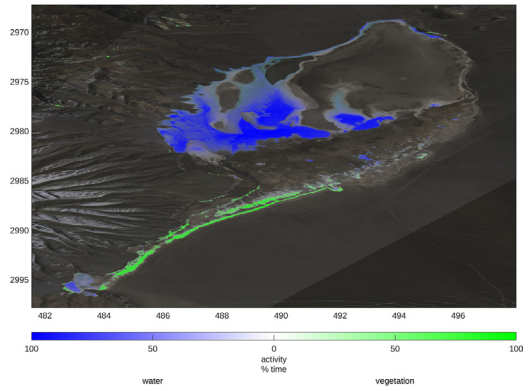

ARTICLE INFO

Article history:
Received 10 August 2020
Received in revised form 16 October 2020
Accepted 3 November 2020
Available online 20 November 2020

Editor: Martin Drews

Keywords:
High Andean wetlands
Water availability
Long-term monitoring
Climate variability
Terminal wetlands

ABSTRACT

High Andean wetlands of the elevated plateaus of the Andes Mountains of Chile, Argentina, Perú and Bolivia are true oases that sustain life in this arid region. Despite their ecological value, they have been rarely studied and are vulnerable to climate change and human activities that require groundwater resources. One such activity that may be intensified in the near future is mining for nonmetallic minerals such as lithium, whose worldwide demand is expected to increase with the rise of electric vehicles that need batteries. To determine a baseline of the natural dynamics of these systems, which allows sustainable management, it is essential to understand the spatiotemporal dynamics of these wetlands. In this article, we studied the temporal and spatial dynamics of high Andean wetlands of Chile, with the aim of identifying the key processes that govern their dynamics. To do this, we used time series of Landsat data from 1984 to 2019 to study 10 high Andean wetlands. Furthermore, to characterize the climate variability in these systems, we studied the long-term relation between the changes in water and vegetation areas with rainfall and evaporation variability. It was found that the groundwater reservoir plays a key role in sustaining the high Andean wetlands. Wet years with a period of occurrence of 20–30 years are the years in which the groundwater reservoirs are actually recharged, and in between wet years, the groundwater reservoirs gradually release the water that sustains the aquatic ecosystems. Hence, groundwater exploitation should be carefully designed from a long-term perspective, as groundwater levels could take decades to recover.

* Corresponding author at: Departamento de Ingeniería Civil, Universidad de Chile, Avda. Blanco Encalada 2002, Santiago 8370449, Chile.
E-mail address: aldelafu@ing.uchile.cl (A. de la Fuente).

https://doi.org/10.1016/j.scitotenv.2020.143830

1. Introduction

High Andean wetlands are found in the elevated plateaus of the Andes Mountains of Chile, Argentina, Perú and Bolivia. These are true oases that sustain life in this arid region. Despite the ecological value of these systems, they have been rarely studied, and paradoxically, they are under threat from the renewable energy revolution, as they have the main deposits of lithium salts in the world, which is an essential mineral for battery manufacturing (Kesler et al., 2012; Munk et al., 2016).

These wetlands are the result of groundwater upwelling that flows into terminal shallow lakes located at the central depression of a closed basin (Risacher et al., 2003; Cabrol et al., 2009; de la Fuente and Niño, 2010). These systems are hydrologically closed basins, as the water that precipitates into the basin is completely evaporated from the soil and the terminal shallow lake of the basin, thus evapo-concentrating the salts up to 250 g l^{-1} (reported in de la Fuente and Niño, 2010), which is why these shallow lakes are called salars (Dorador et al., 2009; de la Fuente and Niño, 2010). Vegetation patches can be found in the perimeter of the shallow lakes, whose distribution responds to local conditions of soil humidity and salinity (Ahumada and Faúndez, 2015; Tölgyesi et al., 2015). These places become important since the vegetation supports different types of fauna that take advantage of these wetlands for drinking, hunting and nesting (Risacher et al., 2003), thus forming ecological hotspots in the Andes Mountains.

Furthermore, these high Andean wetlands in the Altiplano region have tremendous economic value because they contain the main reserves of lithium and several other minerals in the world (Kesler et al., 2012; Munk et al., 2016). Lithium exploitation is based on brine pumping from the groundwater, which reduces the availability of water that upwells into these systems (Marazuela et al., 2019a, 2020), thus producing serious damage to the ecosystem. Therefore, to obtain a baseline of the natural long-term dynamics of these systems, which allows designing sustainable management, it is essential to first understand the long-term spatiotemporal variability in these terminal wetlands, as argued by Wilkinson et al. (2020).

In this article, we hypothesize that spatial and temporal variability of the high Andean wetlands is high, and strongly related to rainfall and evaporation, with groundwater recharge being of major importance. This is an important aspect for the water balance of the endorheic basins not only of the Altiplano but from all the world, as typically it is assumed that the areas of these wetlands are constant, an assumption that not necessarily is valid. Hence, we study the temporal and spatial dynamics of these wetlands in the Altiplano plateau of Chile, with the aim of identifying the key processes that govern their long-term dynamics. To do this, we use time series of Landsat data from 1984 to 2019 to study the 10 high Andean wetlands detailed in Fig. 1. The Landsat satellite products provide reliable data for studying wetlands and are thus extensively used for characterizing long-term temporal changes in water

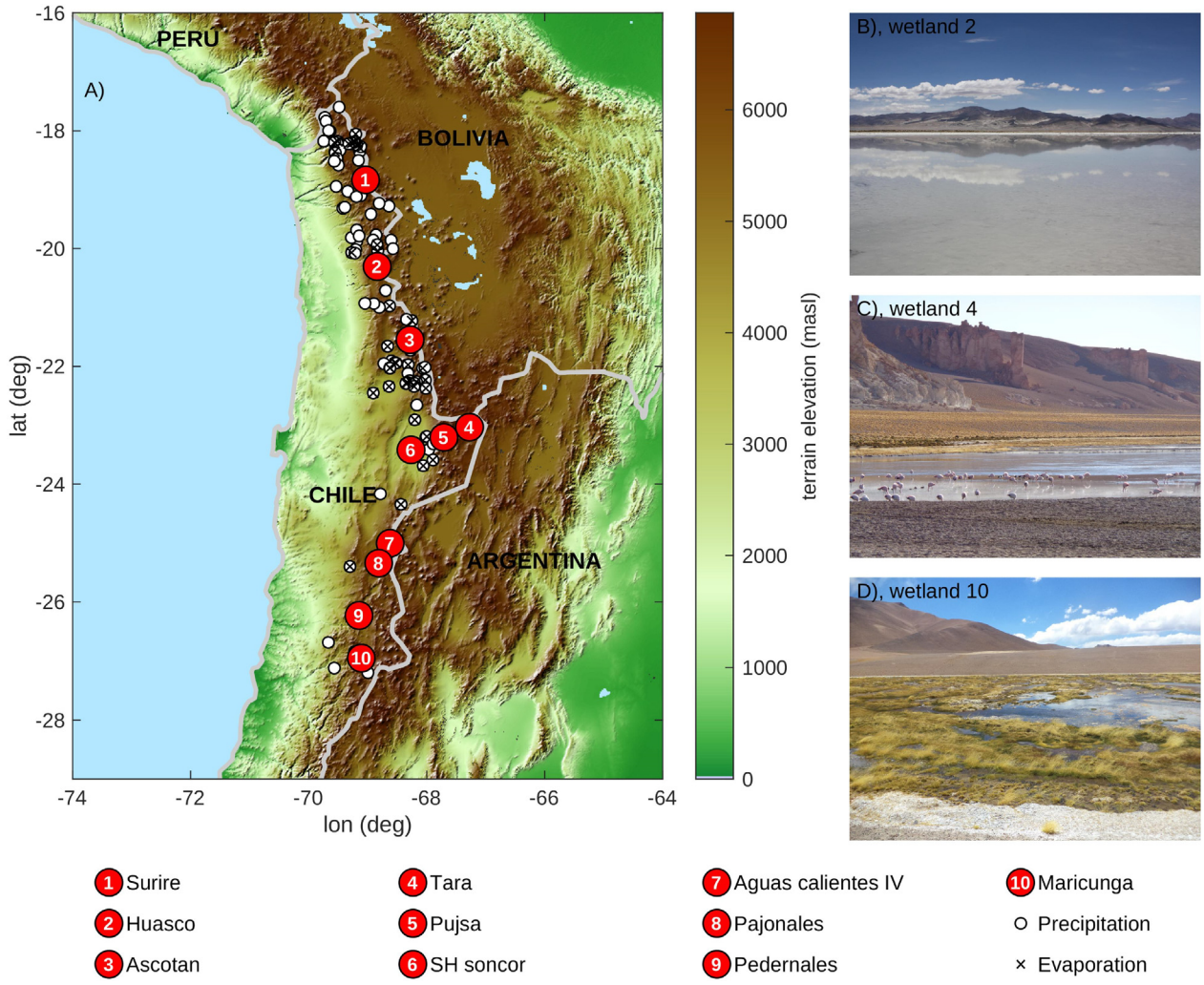

Fig. 1. A) Chilean part of the Altiplano region of the Andes Mountains. Location of selected high Andean wetlands (red circles with numbers) and meteorological stations in the area for precipitation (white circles) and evaporation (black crosses) monitoring. B to D) pictures of wetlands 2, 4 and 10.

and vegetation areas (Bortels et al., 2011; Kayastha et al., 2012; Tulbure and Broich, 2013; Banerjee et al., 2016; Mueller et al., 2016; Bowen et al., 2017). Furthermore, to characterize the climate variability in these systems, we study the long-term relation between the changes in water and vegetation areas with rainfall and evaporation variability. For this, we use the PERSIANN product (Precipitation Estimation from Remotely Sensed Information using Artificial Neural Networks, Nguyen et al. (2019)) for precipitation, and the potential evaporation is computed with the spectral model of de la Fuente and Meruane (2017a, 2017b).

2. Materials and methods

We choose the 10 high Andean wetlands located along the Chilean side of the Altiplano plateau shown in Fig. 1 and listed in Table 1. For each of these wetlands, we characterized the temporal and spatial variation in the areas of the shallow lake and vegetation patches in response to changes in the precipitation and evaporation rates, as detailed below.

2.1. Sizes of shallow lakes and vegetation patches

The sizes of each shallow lake and the surrounding vegetation patches were estimated with Landsat 5 and 8 satellite images, as described below. For this, we obtained a total of 533 images, which correspond to the entire record of Landsat 5 and 8 satellite images: 389 images between May 1984 and June 2013 (Landsat 5) and 144 images between March 2015 and December 2019 (Landsat 8). Each pixel of the satellite images corresponds to a parcel of land of 30 m ×30 m. No satellite information is available between June 2013 and March 2015.

Satellite-derived indices were used as a surrogate of the sizes of the vegetation patches and the shallow lakes. Several satellite-derived indices have been developed for vegetation monitoring, as the spectral reflectance signature reveals information about the state, biogeochemical composition, and structure of a leaf and canopy (Huete, 2012), as well as for surface waters delineation (McFeeters, 1996; Ji et al., 2009; Gao et al., 2012). On one hand, the Normalized Difference Vegetation Index (NDVI) captures the contrast in light reflection from green leaves between the red and the near infrared (NIR) spectral bands, enhancing locations with terrestrial vegetation. Consequently, it was used to delineate vegetation patches and to determine their size. On the other hand, the Normalized Difference Water Index (NDWI) aims to enhance water features (McFeeters, 1996), and thus it was selected to delineate the shallow lakes and its extent. For each pixel of the satellite images, we computed the NDVI and NDWI indexes (Rouse et al., 1973; McFeeters, 1996; Gao, 1996; Guichard et al., 2000), defined as:

$$NDVI = \frac{(NIR - Red)}{(NIR + Red)} \quad ; \quad NDWI = \frac{(GREEN - \mathrm{SWIR})}{(GREEN + \mathrm{SWIR})} \tag{1}$$

where *Red* denotes the red wavelengths, *SWIR* denotes the shortwave infrared and *GREEN* denotes the green wavelength band (Ji et al., 2009). Note that we used the GREEN bandwidth for computing the NDWI because Ji et al. (2009) showed that it provides more stable results than those obtained based on the Near Infrared bandwidth. The NDVI and NDWI indices are dimensionless numbers that take values between −1 and 1, and the adopted methodology for identifying vegetation or open water is to define a threshold value for each index (NDVI and NDWI) such that if the value of the index is larger than this threshold, the pixel is covered with vegetation or water; otherwise, the pixel is empty of vegetation or water (Gao, 1996; Guichard et al., 2000; Ji et al., 2009). The thresholds for each wetland were defined by the manual inspection of satellite images to define the size of the wetland, which was contrasted to the size of the wetland computed based on the NDWI and NDVI indices. The limitation of the adopted methodology are that obtained threshold for delimiting the areas covered with vegetation and water are not unique and varies wetland to wetland, and recent studies showed that the computed NDWI and NDVI indexes varies in time due to orbit drift of the satellites (up to 10% in USA, Roy et al., 2020). Consequently, the impact of the uncertainty of the threshold values on the computed areas was quantified by recomputing the areas of the wetland by changing the threshold value in ±20%. Then, the frequency distribution of the areas of the wetland was computed and used to evaluate how sensible is the obtained areas to changes in the threshold values.

Finally, the analysis for quantifying the temporal variations of the sizes of the shallow lakes and vegetation patches was performed based on computing the percentage of time that each pixel corresponds to vegetation or water. As a consequence, it is possible to identify areas of the wetland that are usually covered with vegetation or water (more than 50% of the time), areas that are temporarily covered by vegetation or open water (more than 16% of the time), and desert areas. A time series of these two characteristic sizes was computed with a moving time window of five years, in which each of these time windows has approximately 70 satellite images. The time window of 5 years was chosen due to its reliable representation of decadal variation (Nyquist's theorem), while keeping a significant number of observations (70 satellite images) for the statistical analysis. Since one of our hypothesis is that the temporal variability of the size of the wetlands is high, the analysis of the temporal evolution of the size of the wetlands is given in terms of the 16% and 50% percentiles of the frequency distribution of the areas within the time window of 5 years. These percentiles are associated to areas of the wetland that are sporadically covered with vegetation or water (less than 16% of the time) and frequently covered with vegetation or water (more than 50% of the time), thus enabling identifying changes in the core of the wetlands and the peripheral area of the wetlands.

2.2. Precipitation and evaporation variability

Daily precipitation and evaporation in the Andes Mountains are regularly measured by the Chilean National Water Agency (DGA, Dirección

Table 1
Identification of the high Andean wetlands chosen for this research. Lat, Lon and Elev denote the coordinates and elevations of the wetlands. The catchment area was obtained from Risacher et al. (2003), *Pp* is the median annual precipitation computed based on the PERSIANN product, and *Ev* is the median annual potential evaporation from de la Fuente and Meruane (2017a, 2017b).

ID	Name	Lat (°S)	Lon (°W)	Elev (masl)	Catchment area (km^2)	P_p (mm/yr)	E_v (mm/yr)
1	Surire	18.834	69.036	4260	574	285	1053
2	Salar del Huasco	20.305	68.839	3778	1572	135	1285
3	Ascotan	21.550	68.283	3716	1757	149	1070
4	Tara	23.033	67.275	4400	2035	228	855
5	Pujsa	23.207	67.710	4500	634	195	848
6	SH Soncor	23.418	68.266	2300	1810	70	957
7	Aguas Calientes IV	25.004	68.621	3665	656	96	1036
8	Pajonales	25.343	68.814	3537	1984	76	1039
9	Pedernales	26.228	69.148	3370	3620	156	1075
10	Maricunga	26.948	69.108	3760	3045	272	865

General de Aguas), with nearly 102 stations in the Altiplano region for precipitation (white circles in Fig. 1) and 42 stations for evaporation (black crosses in Fig. 1). However, not all of these stations have data for the entire time period where Landsat information is available, and some of the chosen high Andean wetlands have no measurements for their corresponding basin. Consequently, we decided to base the analysis on the combination of direct measurements, remote products and indirect methods. Particularly, the PERSIANN product (Precipitation Estimation from Remotely Sensed Information using Artificial Neural Networks, Nguyen et al., 2019) is used for precipitation, and the potential evaporation is computed with the spectral model of de la Fuente and Meruane (2017a, 2017b).

The PERSIANN product has been updated on a daily basis since January 1983 for a worldwide regular grid with information distributed every 0.25°. To validate the use of this remote sensing product for the Altiplano region, the PERSIANN information from the regular grid was spatially interpolated to the location of each DGA station. The comparison between the measured precipitation at the 102 DGA stations and the PERSIANN product is shown in Fig. 2A, where the gray circles denote the mean daily precipitation at each station, and the red triangles denote the average monthly precipitation at all stations. Furthermore, Fig. 2C shows in bars the observed monthly precipitation of all the stations and for three different exceedance probabilities (16%, 50% and 84%), and in red circles the corresponding value of the PERSIANN product. As a consequence, Fig. 2A and C show that the PERSIANN product is capable of reproducing both the spatial distribution of the precipitation and seasonal variability in the Altiplano region, thus validating the use of this product for the purpose of this study. The standard difference between these two sets of information on a daily basis was 0.6 mm.

The potential evaporation is defined as the evaporation that occurs from open water bodies without considering reduction due to water salinity (de la Fuente and Niño, 2010) or the presence of terrestrial vegetation. It was computed with the spectral model of de la Fuente and Meruane (2017a, 2017b), which uses the NCEP-NCAR atmospheric reanalysis as input (Kalnay et al., 1996) and computes the surface energy balance in shallow lakes of the Altiplano region. Similar to Fig. 2A and C, Fig. 2B and D compares the observed and predicted potential evaporation for the 42 DGA stations in the Altiplano region with evaporation measurements. A pan coefficient of 0.65 was used (Risacher et al., 2003; de la Fuente and Meruane, 2017b). Fig. 2B and D shows that the model can reproduce the spatial distribution and seasonal variability in potential evaporation in the Altiplano region; however, the model tends to amplify the seasonal variability in potential evaporation since the simulated potential evaporation are higher than the observation in summer, and smaller than the observations in winter. The standard difference between these two sets of information on a daily basis was 1.1 mm.

The water cycle is closed in endorheic basins of the Altiplano, such that a fraction of the water that precipitates into the catchment is evaporated from the basin, while the rest of the water infiltrates and recharges the groundwater reservoir and then upwells toward the terminal wetland (de la Fuente and Meruane, 2017b; Marazuela et al., 2019a, 2020). Sophisticated models perform a water balance in the vadose zone to quantify the actual groundwater recharge (Uribe et al., 2015); however, as a first approximation, the vadose zone was not included in this article, and we directly estimated the amount of water that actually infiltrates toward the aquifer (herein called groundwater recharge, *GR*) as

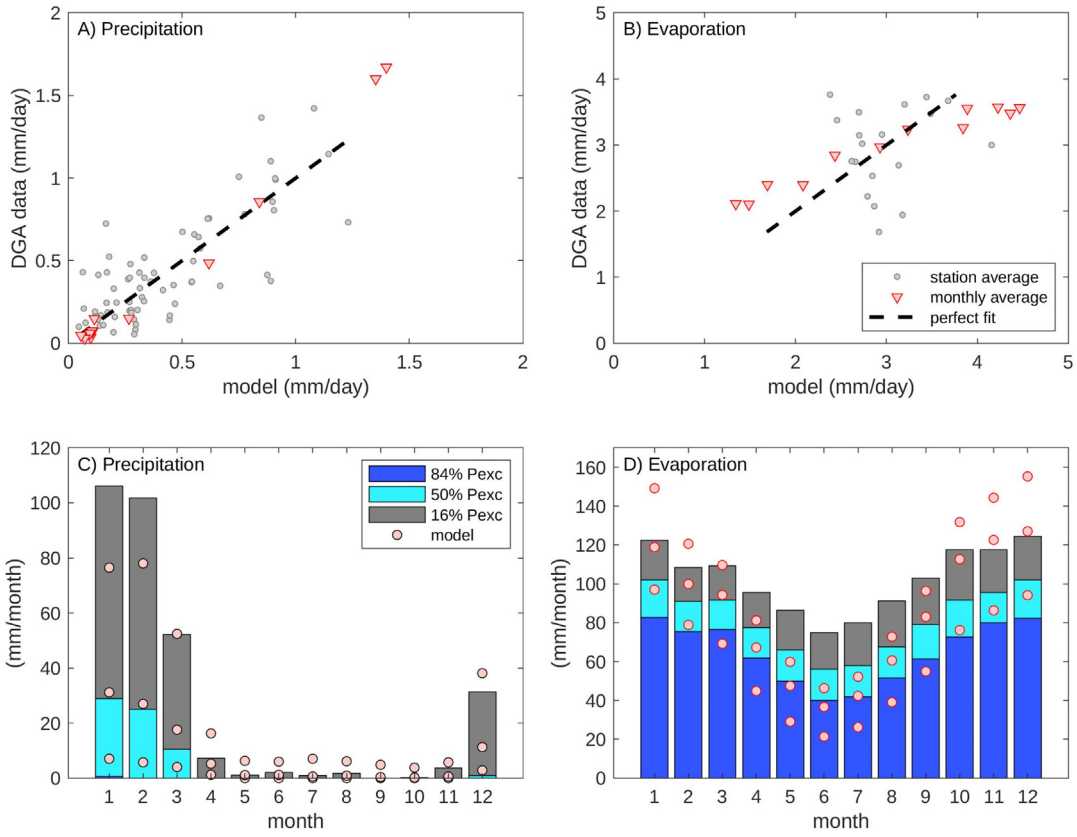

Fig. 2. A) Comparison between the average measured daily precipitation at each DGA meteorological station and the corresponding PERSIANN product (gray circles) and monthly average of all stations (red triangles). B) Similar to A), for the measured potential evaporation and the computed potential evaporation with the spectral model. C) Comparison between measured total monthly precipitation (bars) and the corresponding PERSIANN product (red circles) for different exceedance probabilities (84%, 50% and 16%). D) Similar to C) for potential evaporation.

$$GR = \max\left(P_p - E_v, 0\right) \quad (2)$$

GR was computed based on the daily values of precipitation and potential evaporation, and then the monthly and annual totals were computed; otherwise, *GR* would be equal to 0, as monthly and annual potential evaporation are always larger than the monthly and annual precipitation.

2.3. Normalization of variables

For comparison among the different wetlands, the variables were normalized as

$$X^* = \frac{X - average(X)}{standard deviation(X)} \quad (3)$$

where the subscript * is used to note dimensionless variables and *X* denotes the variable that is normalized (precipitation P_p, groundwater recharge *GR*, area of shallow lakes A_w, or area of vegetation patches A_v). Note that here we used the statistical metrics to understand the temporal fluctuations of the variables. $X^* < 0$ means that the dimensional variable *X* is smaller than the average; and if the absolute value of X^* is smaller than 1, the dimensional variable is within the standard deviation of the time series.

3. Results

3.1. Climatic variability in the water balance

The results for each wetland are shown in Table 2 and Fig. 3. The median annual precipitation for the entire period (1983–2019) ranges from 100 to 300 mm/year (Fig. 3A), while the groundwater recharge is between 10% and 35% of the precipitation (Table 2). Changes in the percentage of groundwater recharge are primarily explained by the total precipitation (Fig. 3B). In particular, the percentage of groundwater recharge increases with the total precipitation, as only the precipitation that exceeds the potential evaporation contributes to groundwater recharge.

Figs. 4 and 5 describe the seasonal evolution of precipitation and groundwater recharge for the studied wetlands. As shown below, the Tropic of Capricorn is used to delimit two classes of terminal wetlands. Fig. 4 shows the time series of the total monthly precipitation and groundwater recharge for wetlands 2 (Salar del Huasco) and 9 (Pedernales) from July 1995 to July 1999. These wetlands are selected as examples as Salar del Huasco is located north of the Tropic of Capricorn, whereas Pedernales is located south of it. Fig. 4 shows that the precipitation in Salar del Huasco (Fig. 4A) is more concentrated in the austral summer (December to April), while it is more difficult to identify seasonal patterns in the precipitation in Pedernales (Fig. 4B). This difference between wetlands 2 and 9 can be attributed to the relative latitude of the wetland with respect to the Tropic of Capricorn, as shown in Fig. 5A, which plots the median total monthly precipitation for all 10 terminal wetlands and was constructed based on the PERSIANN information. As shown in Fig. 5A, precipitation is concentrated during the austral summer (December to March), which is due to humid air advection from the Amazon region (Garreaud et al., 2003). The Tropic of Capricorn, on the other hand, is a limit that allows classifying high Andean wetlands in terms of their seasonal distribution of precipitation: for those located north of the Tropic of Capricorn (with latitudes smaller than 23.5°S), precipitation is concentrated from December to March, while for high Andean wetlands located south of the Tropic of Capricorn, precipitation is more uniformly distributed over the year. On average, for wetlands located north of the Tropic of Capricorn, 74% of precipitation is expected to occur from December to

Table 2
Main results of the study. *GR* is the median annual groundwater recharge computed with Eq. (2) were numbers in brackets corresponds to groundwater recharge of the percentiles 16% and 84%. Columns 4–7 indicate the threshold values of the NDVI and NDWI used to determine the water and vegetation extensions of the Landsat 5 (L5) and Landsat 8 (L8) satellites. *Aw* and *Av* are the areas of water and vegetation computed with the satellite images and the percentages that accompany these variables correspond to percentiles 16%, 50% and 84%. Numbers in round brackets indicates the corresponding area computed with the NDVI and NDWI thresholds ±20%.

ID	Name	*G* (mm/yr)	NDVI L5	NDWI L5	NDVI L8	NDWI L8	$A_{w\ 16\%}$ (km^2)	$A_{w\ 50\%}$ (km^2)	$A_{w\ 84\%}$ (km^2)	$A_{v\ 16\%}$ (km^2)	$A_{v\ 50\%}$ (km^2)	$A_{v\ 84\%}$ (km^2)
1	Surire	65.7 (34.6–91.4)	0.14	0.6	0.21	0.4	4.961 (2.028–8.674)	12.817 (8.472–16.963)	26.482 (19.432–33.429)	0.746 (0.333–1.339)	1.579 (1.095–2.242)	3.367 (2.652–4.345)
2	Salar del Huasco	10.1 (3.8–21.8)	0.05	0.35	0.15	0.29	1.378 (1.100–1.653)	2.251 (1.935–2.681)	3.439 (2.952–4.136)	0.584 (0.327–0.984)	1.262 (0.865–2.219)	3.001 (2.122–5.435)
3	Ascotan	6.4 (2.0–21.1)	0.065	0.2	0.12	0.19	4.791 (3.842–6.257)	18.011 (14.248–22.538)	40.534 (34.562–46.336)	0.031 (0.015–0.070)	0.098 (0.058–0.218)	0.300 (0.150–1.276)
4	Tara	21.3 (7.4–45.0)	0.04	0.8	0.13	0.45	10.576 (8.821–13.218)	16.267 (13.694–20.073)	26.944 (21.840–34.621)	0.148 (0.098–0.218)	0.273 (0.193–0.440)	0.507 (0.366–0.808)
5	Pujsa	71.6 (38.5–130.6)	0.04	0.7	0.11	0.52	2.019 (0.000–15.731)	17.825 (0.002–23.280)	25.153 (0.158–29.635)	0.414 (0.215–0.789)	1.547 (1.173–2.164)	4.108 (3.570–5.032)
6	SH Soncor	54.1 (32.4–103.9)	0.03	0.3	0.11	0.22	1.603 (0.001–3.183)	4.086 (1.185–5.849)	6.674 (3.483–8.671)	0.053 (0.034–0.092)	0.220 (0.174–0.292)	0.620 (0.544–0.703)
7	Aguas Calientes IV	11.0 (4.3–21.6)	0.0095	0.8	0.09	0.5	7.697 (5.550–11.512)	11.902 (8.089–18.581)	19.685 (13.109–30.190)	10.604 (7.400–13.340)	15.955 (11.662–24.413)	24.852 (19.443–40.204)
8	Pajonales	11.2 (3.2–29.3)	0.011	0.3	0.092	0.25	0.830 (0.000–3.624)	2.487 (0.000–5.325)	5.214 (0.005–7.923)	0.043 (0.028–0.064)	0.125 (0.092–0.177)	0.254 (0.220–0.405)
9	Pedernales	7.8 (2.9–27.7)	0.02	0.4	0.095	0.3	3.864 (2.801–5.181)	5.100 (4.020–6.466)	14.295 (11.284–20.091)	3.136 (0.014–13.774)	30.898 (11.908–57.965)	72.028 (58.993–119.108)
10	Maricunga	27.5 (11.7–49.5)	0.02	0.5	0.11	0.45	0.722 (0.539–1.078)	1.646 (1.044–2.695)	5.848 (4.637–8.550)	1.675 (0.273–4.164)	5.790 (2.810–11.439)	11.851 (8.684–28.655)

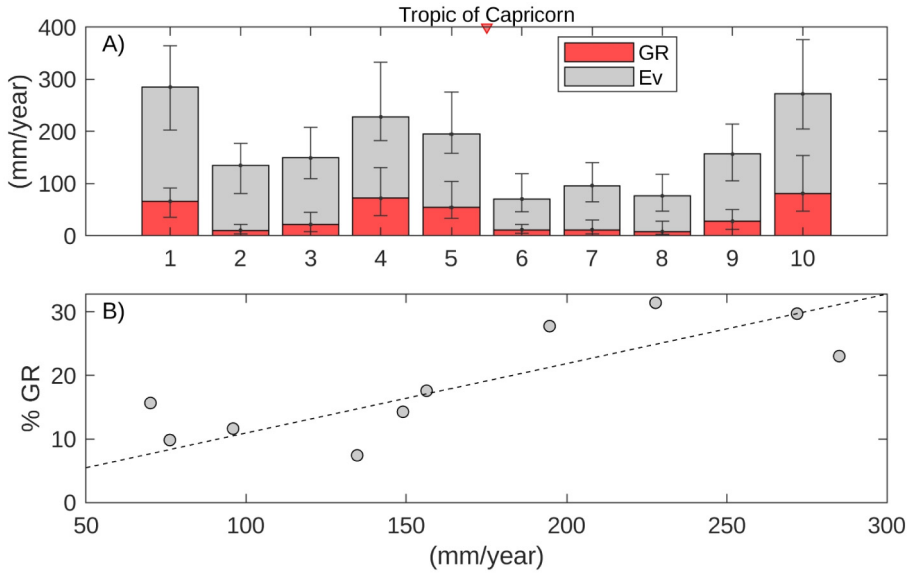

Fig. 3. A) Median annual precipitation for the different high Andean wetlands identified in Fig. 1 and differentiation between the groundwater recharge (red area) and amount of water that is locally evaporated (gray area). Bars define the 84% and 16% percentile. B) Percentage of precipitation that corresponds to the groundwater recharge as a function of the total precipitation.

March, while for those located south of the Tropic of Capricorn, this fraction is reduced to 60%.

In terms of potential evaporation (Fig. 5B and black lines in Fig. 4), maximum values occur in December and January, without significant classification in terms of the latitude of the wetland. The total potential evaporation in a month is always larger than the total precipitation, as shown by the black lines in Fig. 4. However, intense daily precipitation events may result in more precipitation than daily potential evaporation and thus contribute to groundwater recharge in some months, especially in austral autumn, when evaporation is reduced with respect to austral summer. Consequently, in response to the combined seasonal evolution of precipitation and potential evaporation, groundwater recharge is also concentrated during austral summer, as observed from the red bars in Figs. 4 and 5C.

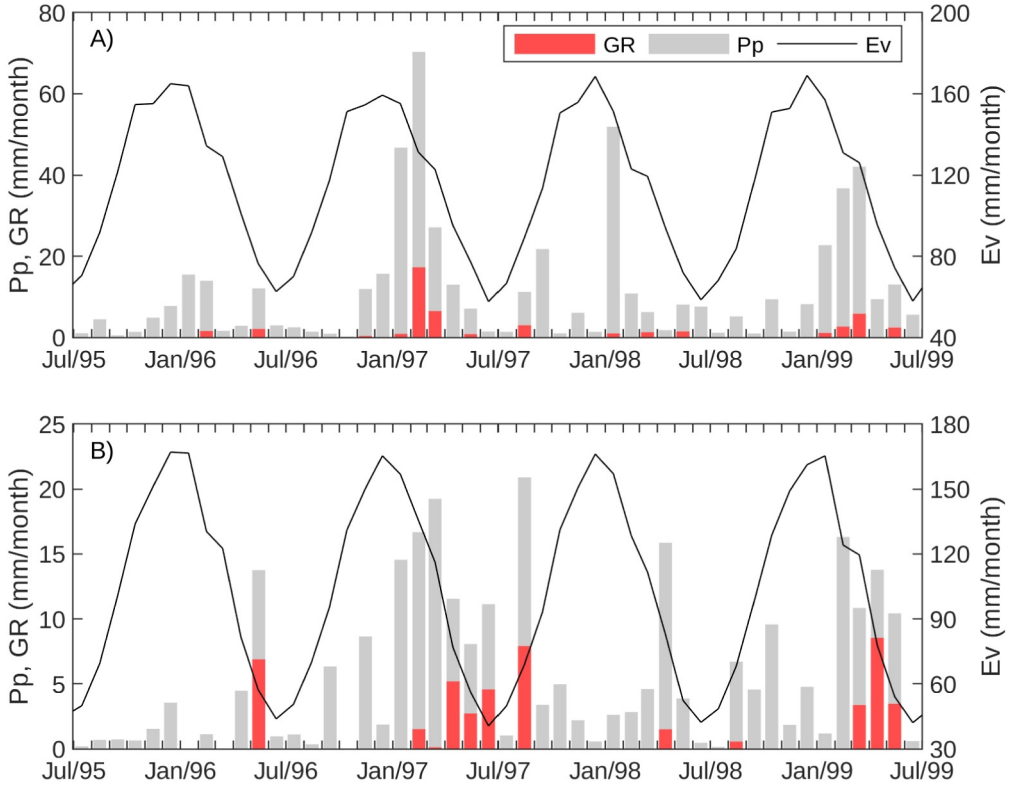

Fig. 4. A) Time series of total monthly precipitation (gray bar), groundwater recharge (red part of the bar) and total potential evaporation (black lines) between July 1995 and July 1999 in wetland 2 (Salar del Huasco). B) Similar to A) for wetland 9 (Pedernales).

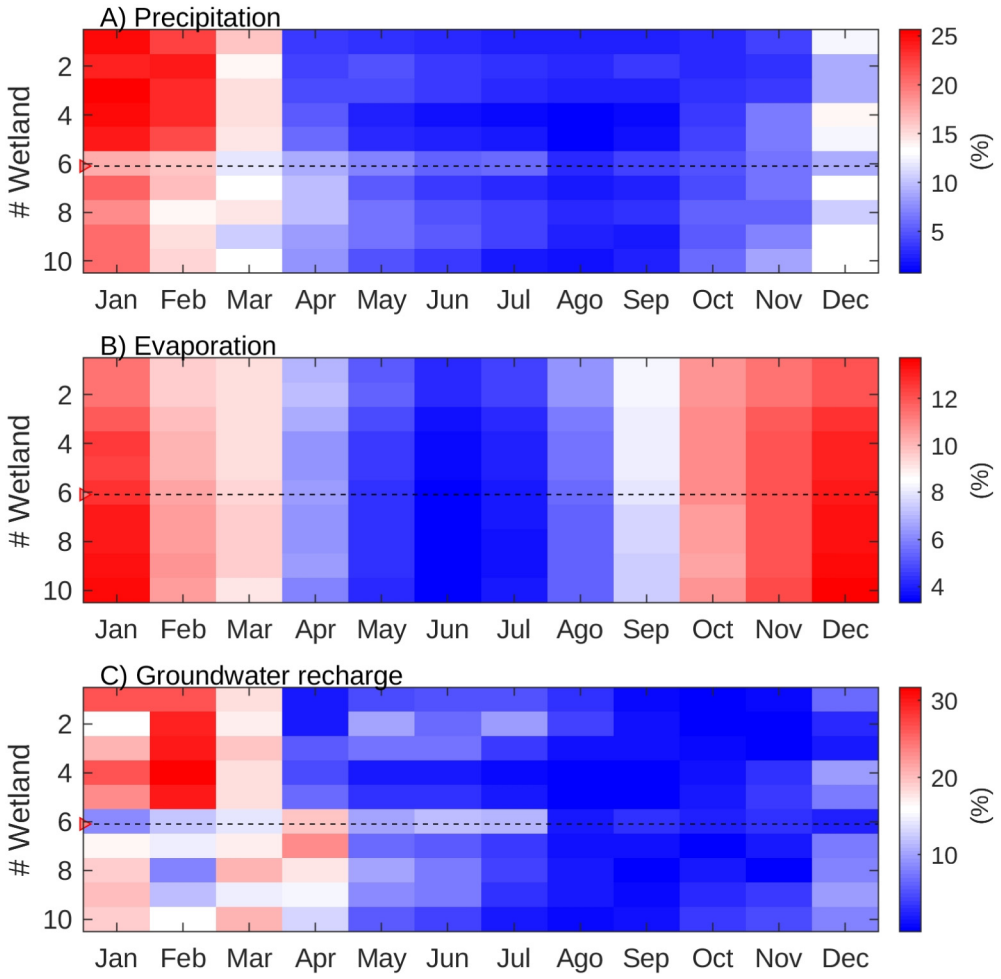

Fig. 5. A) Median total monthly precipitation normalized by the median total annual precipitation. B) Median total monthly evaporation normalized by the mean total annual evaporation. C) Median total monthly groundwater recharge normalized by the mean total annual groundwater recharge. The horizontal dashed line indicates the latitude of the Tropic of Capricorn. (For interpretation of the references to color in this figure, the reader is referred to the web version of this article.)

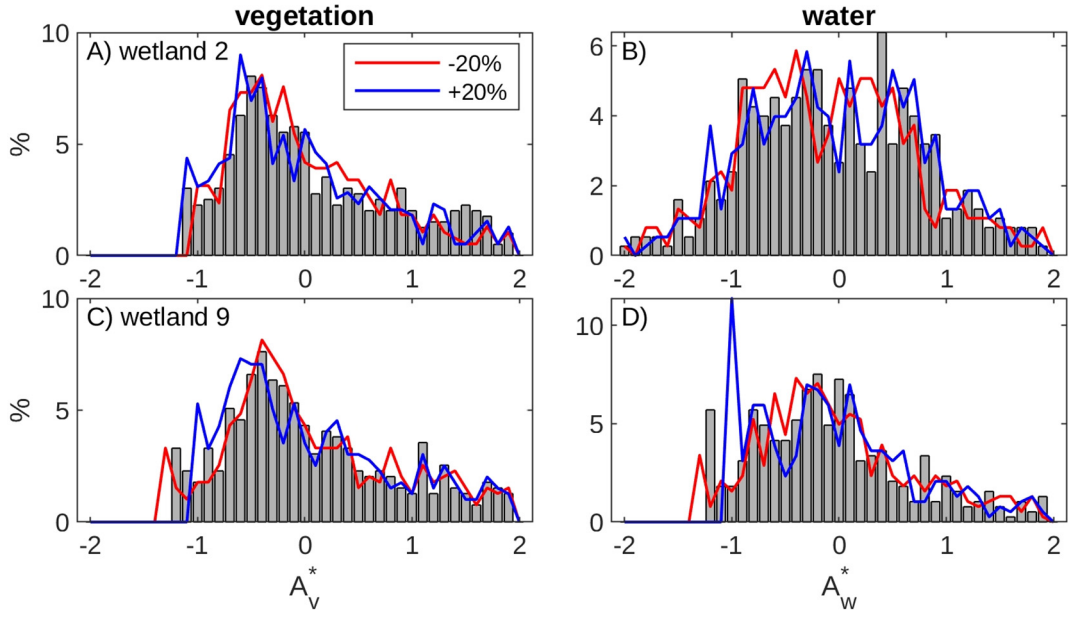

Fig. 6. Frequency distribution of the normalized areas of the wetland obtained with the threshold value of Table 2 (gray bars), and ±20% (blue and red lines). First column is for normalized area of vegetation, and second column for water. First row is for wetland 2 (Salar del Huasco) and second row for wetland 9 (Pedernales).

3.2. Spatial variability in shallow lakes and vegetation patches

Water evaporation occurs in the form of groundwater evaporation from areas where the groundwater is shallow, in the form of direct evaporation from shallow lakes, and in the form of evapotranspiration from vegetation (de la Fuente and Meruane, 2017b). The computed median areas of the shallow lakes and vegetation patches are shown in Table 2, and the sensitivity analysis of the resulting areas is shown in Fig. 6 that plot the frequency distribution of the normalized areas computed with the threshold values of the NDVI and NDWI identified in Table 2 (gray bars), and the frequency distribution of the areas computed with the threshold values ±20% (red and blue lines). In terms of the normalized areas that are here used to quantify the temporal evolution of the size of the wetlands, Fig. 6 shows that the impact of threshold value can be considered small. However, it is important to notice that this conclusion is not valid for dimensional areas listed in Table 2 (not normalized areas shown in Fig. 6) since changes in the threshold value do produce differences in the dimensional area of the wetlands.

In terms of the temporal evolution of the size of wetlands, Fig. 7 plots the percentage of the time that a particular pixel is covered by water (blue) or vegetation (green). Fig. 7 shows that high Andean wetlands are desert oases with a core area that is usually covered with water or vegetation and a peripheral area that is not always covered by water or vegetation.

Seasonal growth and shrinkage dynamics are observed in all the high Andean wetlands studied in this article. Fig. 8 shows the monthly average sizes of the vegetation patches and shallow lakes for wetlands 2 (Salar del Huasco, Fig. 8A) and 9 (Pedernales, Fig. 8B). The sizes of the shallow lakes of these wetlands between 1995 and 1999 (blue bars in Fig. 8) responded to evaporation, with maximum values in the

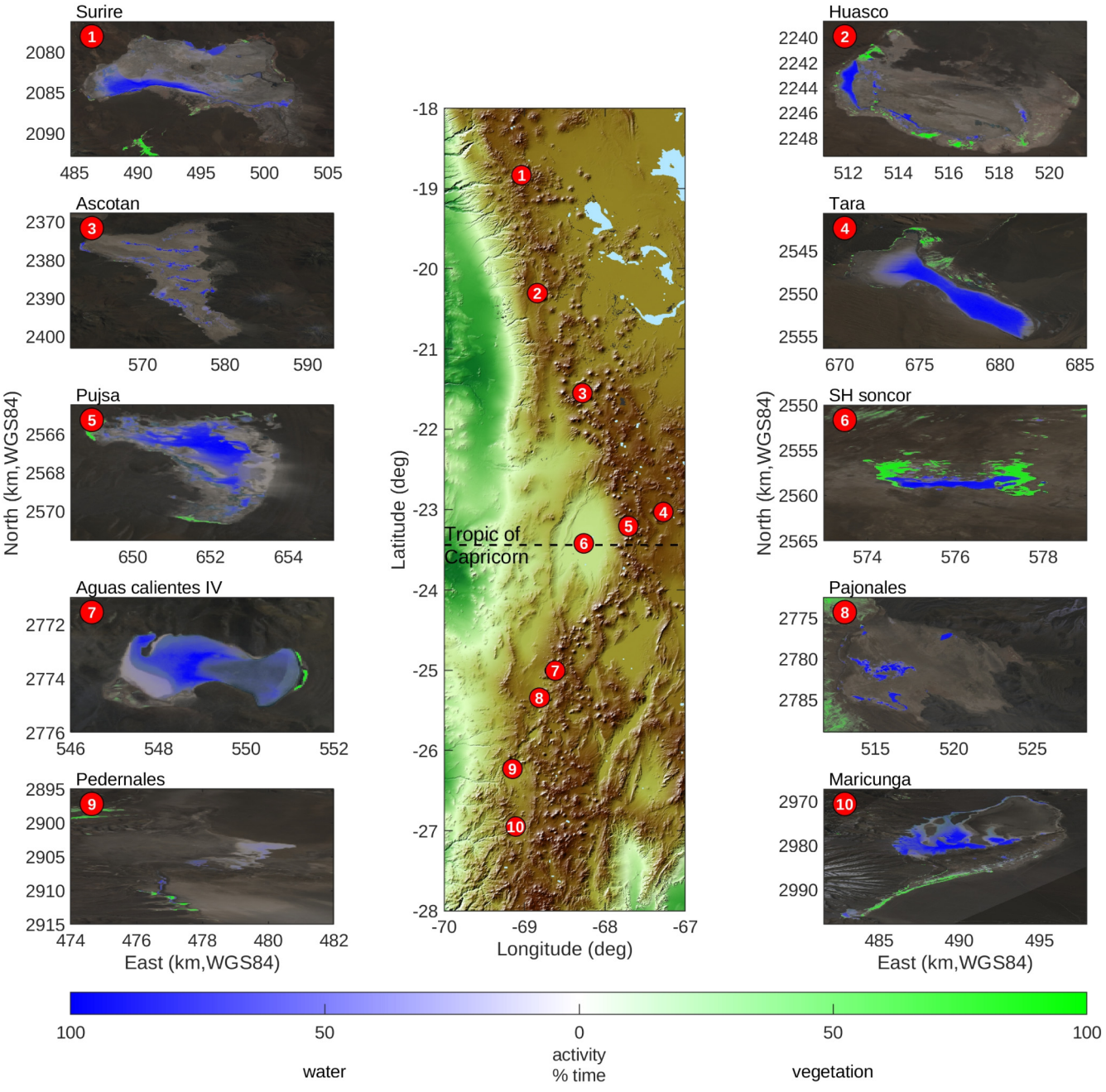

Fig. 7. Satellite images of the studied wetlands; the colour indicates the percentage of the time when a particular pixel is water (blue) or vegetation (green).

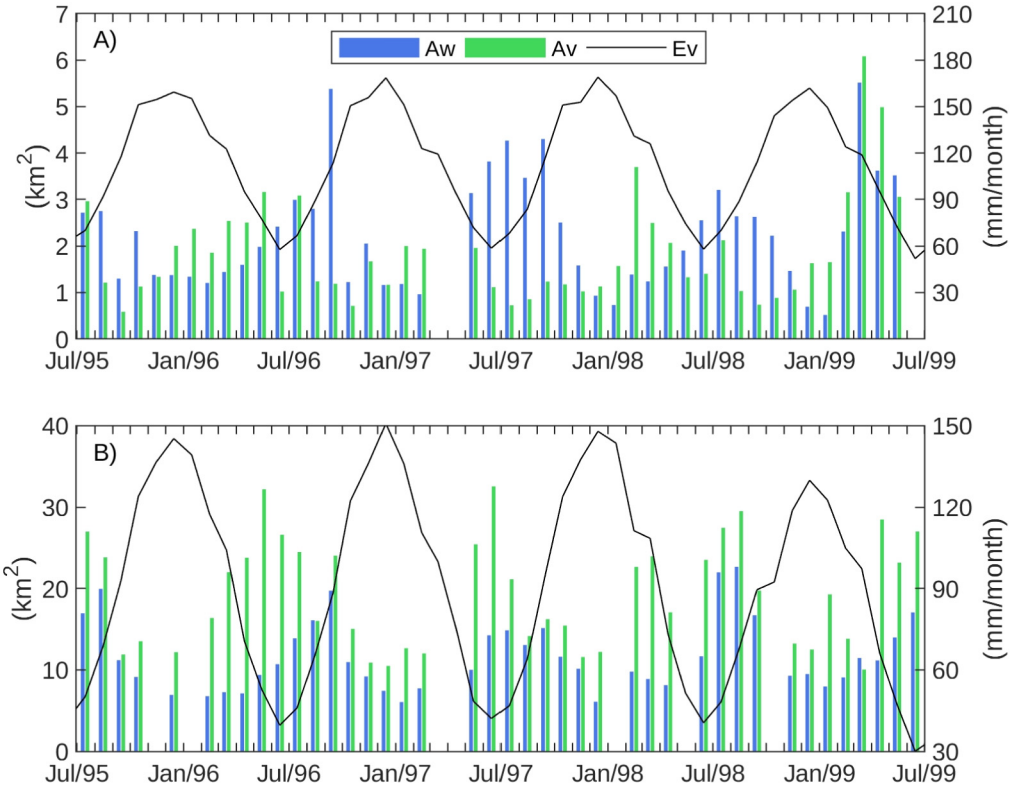

Fig. 8. A) Time series of the size of vegetation (green bars) and shallow lake (blue bars) and total monthly evaporation (black line) of wetland 2 (Salar del Huasco). B) Similar to A) for wetland 9 (Pedernales).

austral winter (July–August, when evaporation is the lowest) and minimum values in summer (December–January, when evaporation is the highest). Moreover, the sizes of vegetation patches also showed seasonal patterns with maximum values in the months from February to April (green bars in Fig. 8) and minimum values in the months from July to September. However, in terms of the vegetation peak, there is one month of delay between the maximum sizes of the vegetation patches in Salar del Huasco and Pedernales.

Fig. 9 plots the normalized size of each wetland (shallow lakes in Fig. 9A and vegetation patches in Fig. 9B) as a function of the month of

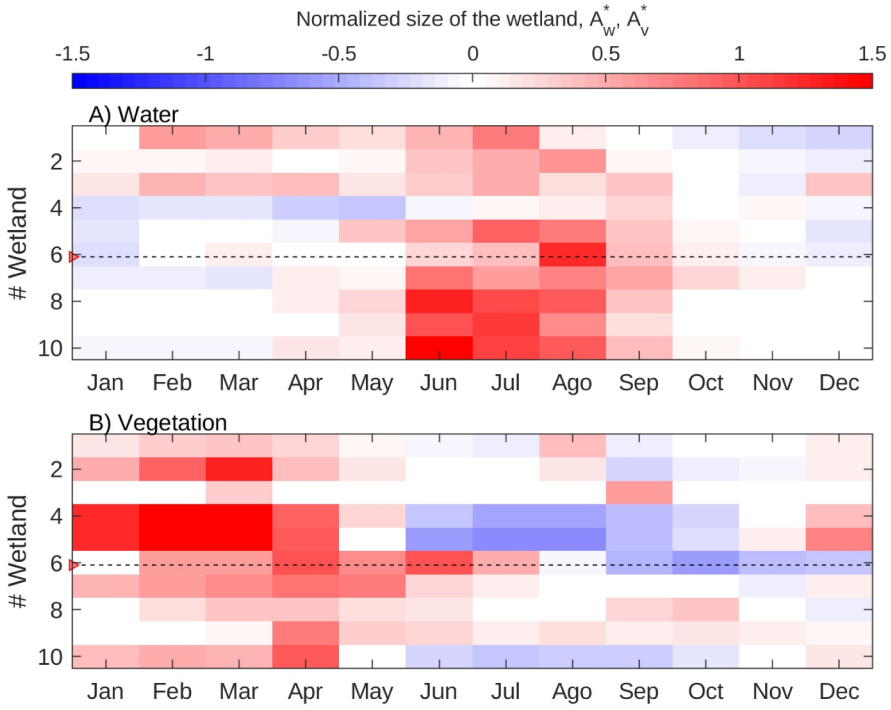

Fig. 9. Normalized size of the shallow lakes and vegetation patches in the wetlands as a function of the month of the year: A) shallow lakes, B) vegetation patches. The horizontal dashed line indicates the latitude of the Tropic of Capricorn.

the year. The largest areas of the wetlands shallow lakes are observed from April to September. In contrast, the largest areas of the vegetation patches are observed from December to May, with peak values from February to March. Once again, differences are observed in terms of the relative location of the wetland to the Tropic of Capricorn: the seasonal changes in the sizes of the shallow lakes are more pronounced south of the Tropic of Capricorn (Fig. 9A), while the size of areas of vegetation tend to be more uniformly distributed throughout the year for the wetlands located south of the Tropic of Capricorn (Fig. 9B).

3.3. Decadal variability in shallow lakes and vegetation patches

The 2D representation of the morphological dynamics observed in the Altiplano region, shown in Fig. 7, enables identification of core areas of the wetland that are frequently covered by water or vegetation, surrounded by other areas that are partially covered in time. Following this spatial classification, the temporal evolution of the size of the terminal wetland was analyzed by computing the surface areas of open water and vegetation that were covered more than 16% and 50% of the time (Fig. 10). To understand the decadal dynamics of the size of shallow lakes and vegetation patches, and its relation with climatic variability, the time series of the ENSO index and of groundwater recharge are presented in Fig. 10A and B. Fig. 10C depicts areas that are sporadically covered by open water bodies, and it shows the existence of shallow lakes with areas larger than the average areas (red colors) in two time periods: after 1985 and after 2001, both during La Niña events (negative ENSO index). While the first time period can be attributed to high groundwater recharge that occurred in the entire region between 1984 and 1985 (Fig. 10A), the second period can be attributed to four years (from 1999 to 2002) with groundwater recharge larger than the average, although less intense than 1984–85. Furthermore, wetlands located north of the Tropic of Capricorn showed a more pronounced response than wetlands located south of the Tropic of Capricorn. Also, a gradual reduction of the area that is persistently covered by open water bodies is observed since 1984 (Fig. 10D), with a small increase for the second period identified in Fig. 10C (after 2001). It is also interesting to note that 2008 was a wet year, with a small increase in the water extension in wetlands located south of the Tropic of Capricorn in 2009. In terms of vegetation patches, both the areas covered with vegetation more than 16% of the time (Fig. 9E) and more than 50% of the time (Fig. 10F) showed a similar response to that observed for open water bodies, but the magnitude of the increase in the area covered by vegetation was not as intense as that observed for open water bodies (Fig. 10C). Finally, it is important to note that in the first years of satellite coverage (since 1984), the areas of the terminal wetlands covered with vegetation patches and open water bodies were smaller than the areas observed in 1985, and this response can be attributed to the intense precipitation that occurred in 1984 and 1985.

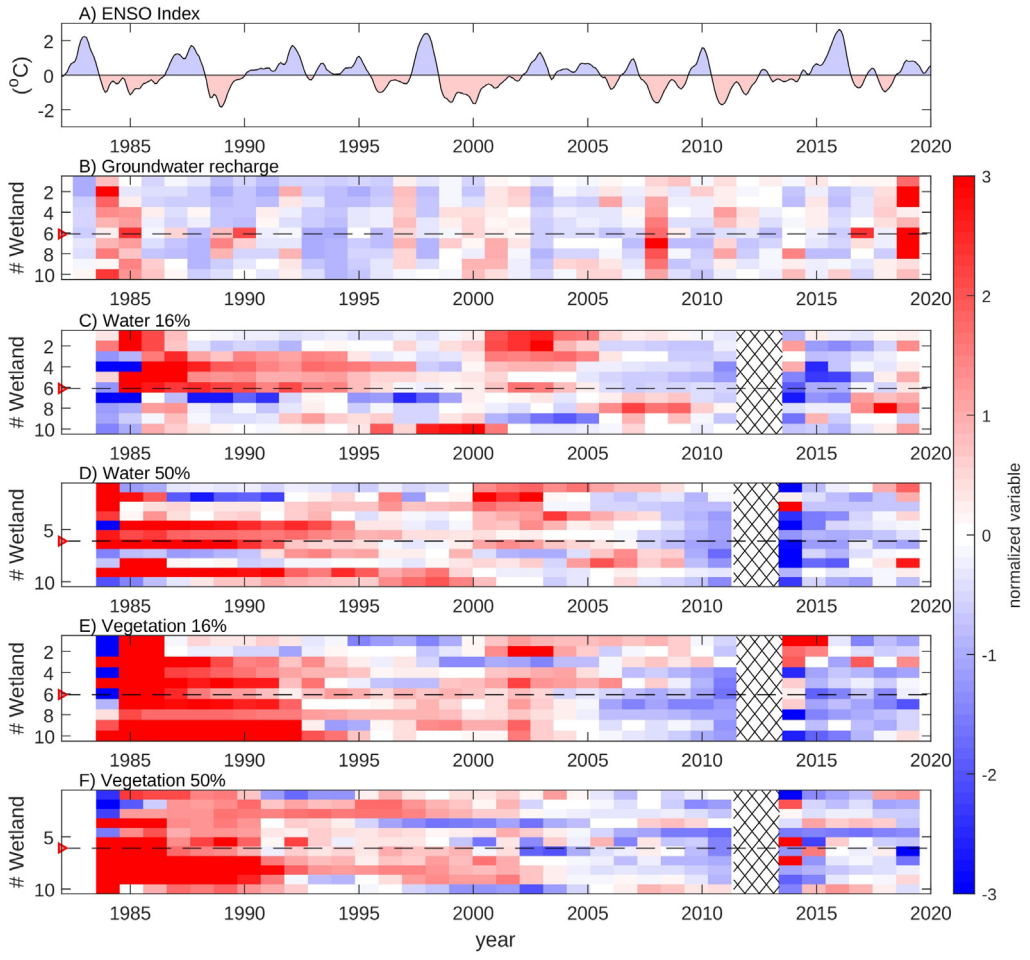

Fig. 10. ENSO index (A) that has been related to the climatic variability in the Altiplano region (Aceituno, 1988, 1989), annual normalized groundwater recharge time series for each wetland sorted by latitude (B), temporal evolution of the normalized area covered by water more than 16% (C) and 50% (D) of the time, and temporal evolution of the normalized size of the vegetation patches that are active more than 16% (E) and 50% (F) of the time. Groundwater recharge and water- and vegetation-covered areas were normalized using Eq. (3). The horizontal dashed line indicates the latitude of the Tropic of Capricorn.

4. Discussion

Our results validate the hypothesis of this article, in which we expected to see high spatial and temporal variability in the high Andean wetlands, which is strongly related to rainfall and evaporation, with groundwater recharge being of major importance. Particularly, our results suggest that the spatiotemporal variability in high Andean wetlands is regulated by the groundwater reservoir, and modulated by seasonal changes in the evaporation, the latitudinal seasonal distribution of precipitation within the year and by their climatic variability due to the El Niño Southern Oscillation (ENSO). In the following subsection, we discuss about these aspects, as well as the implications that this high temporal variability has on closing the hydrological cycle and the water and soil salinity of these wetlands..

4.1. Latitudinal variability in high Andean wetlands

The information analyzed in the article shows that there are some important differences between high Andean wetlands located north of the Tropic of Capricorn and those located south of it. In general, the main difference between these wetlands is the distribution of precipitation within the year. Although to the north of the Tropic of Capricorn, precipitation is expected to occur mainly between December and March, to the south of the Tropic of Capricorn, precipitation is more uniformly distributed throughout the year. This difference is due to the general atmospheric circulation that produces that precipitation regime, which is associated with convective precipitation from humid air advection from the Amazon basin during the austral summer north of the Tropic of Capricorn, while the area south of the Tropic of Capricorn became more important for the influence of frontal rains that reach the continent from the southwest during the austral winter (Aceituno, 1988, 1989; Stull, 1988).

4.2. Temporal variability in high Andean wetlands

It can be inferred that the dynamics describing the size of the high Andean wetlands in the Altiplano region of Chile are driven by a sequence of infrequent wet years followed by several years without significant precipitation rather than a consistent condition, and wetlands grow and shrink in response to seasonal changes in evaporation, as described in Figs. 8 and 9. Under this scheme, the role of the groundwater reservoir is crucial in the dynamics of wetlands, as it stores large volumes of water that enters the reservoir in wet years and gradually releases the water during dry years, sustaining the terminal wetlands. This behavior is better observed in Fig. 11A, which shows the normalized total precipitation based on direct measurements in all the DGA meteorological stations identified in Fig. 1 (black line is the average of the gray lines). In Fig. 11A the red areas depict the periods identified in Fig. 9 where the size of the wetlands was larger than the average (1985–1990 and 2001–2005). Note that 95% of the meteorological stations used in this analysis are located north of the Tropic of Capricorn. Fig. 11A shows that the increase in the sizes of the terminal wetlands in response to the total precipitation is only observed after the wet years 1984–85 and 1999–2001. Recall that no satellite information is available to infer if the wet years of 2012–2013 also resulted in an increase in the size of the terminal wetlands.

The period of occurrence of wet years, on the other hand, which is associated with an increase in the size of a terminal wetland (normalized annual precipitation, $Pp^* \gtrsim 1$), ranges between 15 and 20 years. The frequency distribution of Pp^* is not normal or symmetric but asymmetric (Fig. 11B), such that the median precipitation is $Pp^* = -0.21$. Moreover, the occurrence of wet years with net precipitation larger than the average ($Pp^* > 0$) is less frequent than the dry years with $Pp^* < 0$, and the wettest years correspond to precipitation values up to 4 times the standard deviation of the series with respect to its average ($Pp^* \approx +4$), while the driest years have extreme values of $Pp^* \approx -2$.

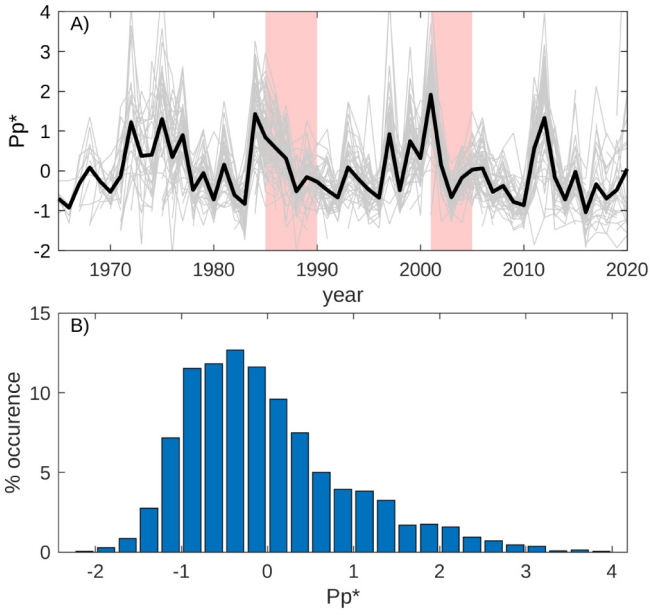

Fig. 11. A) Time series of normalized annual precipitation (Pp^*) measured by 102 stations in the area (gray lines) and average value (thick black line). Red areas indicate period of the time where the size of the wetlands was larger than the average. B) Frequency distribution of Pp^* at all of the meteorological stations in the region.

This statistical description suggests that groundwater recharge is infrequent, and wet years with a period of recurrence of 20 to 30 years are the years in which the groundwater reservoirs that feed the terminal wetlands are actually recharged. Between wet years, the size of a wetland gradually decreases as the inflow discharge is reduced. However, it is important to note that groundwater recharge due to glacier melting should also be added and becomes important in dry years. Therefore, the groundwater reservoir plays a key role in sustaining the high Andean wetlands. This means that the exploitation of these systems based on groundwater extractions should be carefully designed from a long-term perspective, as the groundwater level could take several decades to recover. A similar analysis has been presented for high Andean wetlands in Perú (Mazzarino and Finn, 2016; Pauca-Tanco et al., 2020), where a persistent increase in the size of terrestrial vegetation was reported for two of these wetlands in the satellite Landsat 5. Unfortunately, these trends were not possible to be identified in our analysis.

4.3. Soil and water salinity

The interactions among freshwater recharge, groundwater levels and evaporation rates produce strong water and salinity gradients in the wetlands, which significantly affect the spatial distribution of terrestrial and aquatic biota (Wetzel, 2001; Mitsch and Gosselink, 2015). On one hand, de la Fuente and Niño (2010) showed that water salinity increases with the distance to the groundwater spring that feeds the saline lake, in response to the balance between salt advection, evapoconcentration and salt precipitation. Therefore, dynamic changes in the size of the saline lake may also produce important temporal changes in the salinity distribution within the saline lakes, and conversely to the aquatic biota that feed the birds (Hulbert and Chang, 1983; Mascitti and Kravetz, 2002; Angel et al., 2016). On the other hand, the spatial distribution of terrestrial vegetation species in high Andean wetlands has been related to soil humidity (hydrophilic to halophilic vegetation) and salinity (Ahumada and Faúndez, 2015). Based on these two criteria, the vegetation types of high Andean wetlands are classified as bofedal, pajonal or vega, together with their saline and non-saline variants (Ahumada and Faúndez, 2015). Therefore, changes in soil humidity

and salinity could generate changes in the structure of vegetation patches in the perimeter of the wetlands; for example, it has been shown that small variations on the water table has produced changes on the vegetation species, thus finding xerophytic species where previously hydrophilic species were found (Tölgyesi et al., 2015). These changes occurred in the long-term, when the species cannot acclimatize to the new conditions that are permanent in time, which is different from the natural variability of growth and shrink of wetlands.

Finally, it is important to contextualize that all of the wetland-scale processes associated to the salt transport in the wetlands, are integrated to the hydrogeological salt transport processes in the entire basin (Tejeda et al., 2003; Vásquez et al., 2013; Marazuela et al., 2018, 2019b). Similarly to the hydrological closed cycle in these basins, the salt transport cycle is also closed in the context that there is no external source/sink of salt to/from the basin. Therefore, the salt that enters to the wetland is salt that primarily was diluted from the soil/rock of the basin (the salinity of rainwater can be assumed 0). Furthermore, the inflow mass of salt into the wetland is evapo-concentrated and then precipitates forming the characteristic crust of salt of these wetlands (de la Fuente and Niño, 2010). As a consequence of this hydrogeological cycle of salt transport, the gradual increase of soil salinity may be expected in the geological scale.

4.4. Hydrological cycle in closed basins

The hydrological cycle in closed basins is known such as the long-term balance between precipitation and evaporation is a constraint. Therefore, the terminal wetland is the place where the groundwater recharge is evaporated, and the resulting size of the wetland is the size that enables the complete evaporation of all of the groundwater that upwells in the perimeter of the wetland (de la Fuente and Niño, 2010). Because of this, seasonal changes in the size of the wetland can be linked to seasonal changes in the evaporation (i.e. higher evaporation rates require smaller areas to evaporate the same inflow), and the long-term reduction of the size of the wetland in dry year is linked to the depletion of the groundwater reservoir. Therefore, we showed that a constant area is not a reasonable assumption, neither for the seasonal time scale nor for the decadal time scale. The actual rate per unit of surface area at which the water is transported into the atmosphere should be studied in detail in further studies, such as those performed by Suárez et al. (2020), as well as quantifying the role of groundwater evaporation in the hydrological cycle in endorheic basins of this Andean region (Costelloe et al., 2009; Johnson et al., 2010; Hernández-López et al., 2016). A conclusion that can be obtained from this dynamic is that any permanent groundwater extraction in the basin will eventually produce a permanent decline in the size of the terminal wetland. Therefore, the management of these wetlands with conservation purposes should include the entire basin, and not only the vicinity of the wetland.

Finally, the role that the size of the terminal wetland plays in closing the hydrological cycle is not only restricted to the high Andean wetlands studied in this article. In fact, high Andean wetlands are also known as playas or salt flats landscapes, which can be widely found in the World in places were the annual evaporation exceeds the annual precipitation (Yechieli and Wood, 2002; Kampf et al., 2005). In these type of terminal lakes whose size is dynamically determined by the complete evaporation of the inflow, the long-term monitory of their sizes can be a valuable remote perception tool that would reflect changes in surface and groundwater extraction for human activity, as well as reflecting the impact of climate change on precipitation or evaporation rates.

5. Summary and conclusions

In this article, we use remote sensing to study the spatiotemporal variability in high Andean wetlands in northern Chile. These aquatic ecosystems are vulnerable to climate change and to human economic activities that require groundwater resources, such as mining for nonmetallic minerals (e.g., lithium) whose worldwide demand is expected to increase in the near future. To determine a baseline of the natural dynamics of these systems, which allows sustainable management, it is essential to understand the spatiotemporal dynamics of these wetlands.

Our analyses focused on characterizing the past long-term variability in 10 high Andean wetlands located in the Altiplano plateau of Chile. To do this, we described the climate variability in terms of groundwater recharge. This variable needed to be computed on a daily basis, as the monthly and annual potential evaporation results always exceed the monthly and annual precipitation results in this arid region. Furthermore, we characterized the temporal and spatial variability in these systems by studying the entire record of Landsat satellite images from 1984 to 2019. We showed that the spatiotemporal variability in high Andean wetlands is modulated by the latitudinal seasonal distribution of precipitation within the year and by their climatic variability due to the El Niño Southern Oscillation (ENSO). Because of the latitudinal seasonal distribution of precipitation, wetlands located north of the Tropic of Capricorn have more seasonal variability in their size than wetlands located south of the tropics. Furthermore, the climatic variability in the rain due to ENSO results in the spatiotemporal variability in the size of the wetlands. In years with la Niña events (negative ENSO index), the area of wetlands increases, and this is more pronounced in wetlands located north of the Tropic of Capricorn.

CRediT authorship contribution statement

Alberto de la Fuente: Conceptualization, Methodology, Software, Formal analysis, Writing - original draft, Writing - review & editing, Visualization. **Carolina Meruane:** Conceptualization, Methodology, Writing - original draft, Writing - review & editing, Visualization. **Francisco Suarez:** Methodology, Writing - original draft, Writing - review & editing, Visualization.

Declaration of competing interest

The authors declare that they have no known competing financial interests or personal relationships that could have appeared to influence the work reported in this paper.

Acknowledgments

This article was financed by project FONDECYT, number 1181222. F. Suárez acknowledges support from ANID/FONDECYT/1170850, CEDEUS – ANID/FONDAP/15110020 and CEGA – ANID/FONDAP/15090013.

References

Aceituno, P., 1988. On the functioning of the Southern Oscillation in the South American sector. Part I: surface climate. Mon. Weather Rev. 116. https://doi.org/10.1175/1520-0493(1988)116<0505:OTFOTS>2.0.CO;2.

Aceituno, P., 1989. On the functioning of the Southern Oscillation in the South American Sector. Part II. Upper-air circulation. J. Clim. 2. https://doi.org/10.1175/1520-0442(1989)002<0341:otfots>2.0.co;2.

Ahumada, M., Faúndez, L., 2015. Guía descriptiva de los sistemas vegetacionales azonales hídricos terrestres de la ecorregión altiplánica (SVAHT).

Angel, A., Vila, I., Herrera, V., 2016. Extremophiles: photosynthetic systems in a high-altitude saline basin (Altiplano, Chile). Int. Aquat. Res. 8. https://doi.org/10.1007/s40071-016-0121-6.

Banerjee, B.P., Raval, S., Timms, W., 2016. Evaluation of rainfall and wetland water area variability at Thirlmere Lakes using Landsat time-series data. Int. J. Environ. Sci. Technol. https://doi.org/10.1007/s13762-016-1018-z.

Bortels, L., Chan, J.C.W., Merken, R., Koedam, N., 2011. Long-term monitoring of wetlands along the Western-Greek Bird Migration Route using Landsat and ASTER satellite images: Amvrakikos Gulf (Greece). J. Nat. Conserv. https://doi.org/10.1016/j.jnc.2011.01.004.

Bowen, B.B., Kipnis, E.L., Raming, L.W., 2017. Temporal dynamics of flooding, evaporation, and desiccation cycles and observations of salt crust area change at the Bonneville Salt Flats, Utah. Geomorphology https://doi.org/10.1016/j.geomorph.2017.09.036.

Cabrol, N.A., Grin, E.A., Chong, G., et al., 2009. The high-lakes project. J. Geophys. Res. Biogeosci. 114. https://doi.org/10.1029/2008JG000818 n/a-n/a.
Costelloe, J.F., Irvine, E.C., Western, A.W., Herczeg, A.L., 2009. Groundwater recharge and discharge dynamics in an arid-zone ephemeral lake system, Australia. Limnol. Oceanogr. 54. https://doi.org/10.4319/lo.2009.54.1.0086.
de la Fuente, A., Meruane, C., 2017a. Dimensionless numbers for classifying the thermodynamics regimes that determine water temperature in shallow lakes and wetlands. Environ. Fluid Mech., 1–18 https://doi.org/10.1007/s10652-017-9536-x.
de la Fuente, A., Meruane, C., 2017b. Spectral model for long-term computation of thermodynamics and potential evaporation in shallow wetlands. Water Resour. Res. 53, 7696–7715. https://doi.org/10.1002/2017WR020515.
de la Fuente, A., Niño, Y., 2010. Temporal and spatial features of the thermohydrodynamics of shallow salty lagoons in northern Chile. Limnol. Oceanogr. 55, 279–288. https://doi.org/10.4319/lo.2010.55.1.0279.
Dorador, C., Meneses, D., Urtuvia, V., Demergasso, C., Vila, I., Witzel, K.-P., Imhoff, J.F., 2009. Diversity of *Bacteroidetes* in high-altitude saline evaporitic basins in northern Chile. J. Geophys. Res. Biogeosci. 114. https://doi.org/10.1029/2008JG000837 n/a-n/a.
Gao, B., 1996. NDWI—a normalized difference water index for remote sensing of vegetation liquid water from space. Remote Sens. Environ. 58, 257–266. https://doi.org/10.1016/S0034-4257(96)00067-3.
Gao, K., Xu, J., Zheng, Y., Ke, C., 2012. Measurement of benthic photosynthesis and calcification in flowing-through seawater with stable carbonate chemistry. Limnol. Ocean. Methods 10, 555–559.
Garreaud, R., Vuille, M., Clement, A.C., 2003. The climate of the Altiplano: observed current conditions and mechanisms of past changes. Palaeogeogr. Palaeoclimatol. Palaeoecol. 194. https://doi.org/10.1016/S0031-0182(03)00269-4.
Guichard, F., Bourget, E., Agnard, J.P., 2000. High-resolution remote sensing of intertidal ecosystems: a low-cost technique to link scale-dependent patterns and processes. Limnol. Oceanogr. 45. https://doi.org/10.4319/lo.2000.45.2.0328.
Hernández-López, M.F., Braud, I., Gironás, J., Suárez, F., Muñoz, J.F., 2016. Modelling evaporation processes in soils from the Huasco salt flat basin, Chile. Hydrol. Process. 30, 4704–4719. https://doi.org/10.1002/hyp.10987.
Huete, A.R., 2012. Vegetation indices, remote sensing and forest monitoring. Geogr. Compass 6. https://doi.org/10.1111/j.1749-8198.2012.00507.x.
Hulbert, S., Chang, C., 1983. Ornitholimnology: effects of grazing by Andean flamingo (*Phoenicoparrus andinus*). Proc. Natl. Acad. Sci. U. S. A. 80, 4966–4969.
Ji, L., Zhang, L., Wylie, B., 2009. Analysis of dynamic thresholds for the normalized difference water index. Photogramm. Eng. Remote Sensing 75. https://doi.org/10.14358/PERS.75.11.1307.
Johnson, E., Yáñez, J., Ortiz, C., Muñoz, J., 2010. Evaporation from shallow groundwater in closed basins in the Chilean *Altiplano*. Hydrol. Sci. J. 55, 624–635. https://doi.org/10.1080/02626661003780458.
Kalnay, E., Kanamitsu, M., Kistler, R., et al., 1996. The NCEP/NCAR 40-year reanalysis project. Bull. Am. Meteorol. Soc. 77, 437–471. https://doi.org/10.1175/1520-0477(1996)077<0437:TNYRP>2.0.CO;2.
Kampf, S., Tyler, S., Ortiz, C., Muñoz, J., Adkins, P., 2005. Evaporation and land surface energy budget at the Salar de Atacama, Northern Chile. J. Hydrol. 310, 236–252.
Kayastha, N., Thomas, V., Galbraith, J., Banskota, A., 2012. Monitoring wetland change using inter-annual landsat time-series data. Wetlands https://doi.org/10.1007/s13157-012-0345-1.
Kesler, S.E., Gruber, P.W., Medina, P.A., Keoleian, G.A., Everson, M.P., Wallington, T.J., 2012. Global lithium resources: relative importance of pegmatite, brine and other deposits. Ore Geol. Rev. 48. https://doi.org/10.1016/j.oregeorev.2012.05.006.
Marazuela, M.A., Vázquez-Suñé, E., Custodio, E., Palma, T., García-Gil, A., Ayora, C., 2018. 3D mapping, hydrodynamics and modelling of the freshwater-brine mixing zone in salt flats similar to the Salar de Atacama (Chile). J. Hydrol. 561. https://doi.org/10.1016/j.jhydrol.2018.04.010.
Marazuela, M.A., Vázquez-Suñé, E., Ayora, C., García-Gil, A., Palma, T., 2019a. The effect of brine pumping on the natural hydrodynamics of the Salar de Atacama: the damping capacity of salt flats. Sci. Total Environ. https://doi.org/10.1016/j.scitotenv.2018.11.196.
Marazuela, M.A., Vázquez-Suñé, E., Ayora, C., García-Gil, A., Palma, T., 2019b. Hydrodynamics of salt flat basins: the Salar de Atacama example. Sci. Total Environ. 651. https://doi.org/10.1016/j.scitotenv.2018.09.190.
Marazuela, M.A., Vázquez-Suñé, E., Ayora, C., García-Gil, A., 2020. Towards more sustainable brine extraction in salt flats: learning from the Salar de Atacama. Sci. Total Environ. https://doi.org/10.1016/j.scitotenv.2019.135605.
Mascitti, V., Kravetz, F.O., 2002. Bill morphology ofSouth American flamingos. Condor 104, 73–83.
Mazzarino, M., Finn, J.T., 2016. An NDVI analysis of vegetation trends in an Andean watershed. Wetl. Ecol. Manag. 24. https://doi.org/10.1007/s11273-016-9492-0.
McFeeters, S.K., 1996. The use of the Normalized Difference Water Index (NDWI) in the delineation of open water features. Int. J. Remote Sens. 17. https://doi.org/10.1080/01431169608948714.
Mitsch, W.J., Gosselink, J.G., 2015. Wetlands Fifth Edition.
Mueller, H., Hamilton, D.P., Doole, G.J., 2016. Evaluating services and damage costs of degradation of a major lake ecosystem. Ecosyst. Serv. https://doi.org/10.1016/j.ecoser.2016.02.037.
Munk, L.A., Hynek, S.A., Bradley, D., Boutt, D.F., Labay, K., Jochens, H., 2016. Lithium brines: a global perspective. Rev. Econ. Geol. 18.
Nguyen, P., Shearer, E.J., Tran, H., et al., 2019. The CHRS Data Portal, an easily accessible public repository for PERSIANN global satellite precipitation data. Sci. Data 6, 180296. https://doi.org/10.1038/sdata.2018.296.
Pauca-Tanco, A., Ramos-Mamani, C., Luque-Fernández, C.R., Talavera-Delgado, C., Villasante-Benavides, J.F., Quispe-Turpo, J.P., Villegas-Paredes, L., 2020. Análisis espacio temporal y climático del humedal altoandino de Chalhuanca (Perú) durante el periodo 1986–2016. Rev. Teledetección. https://doi.org/10.4995/raet.2020.13325.
Risacher, F., Alonso, H., Salazar, C., 2003. The origin of brines and salts in Chilean salars: a hydrochemical review. Earth-Sci. Rev. 63, 249–293.
Rouse, J.W., Haas, R.H., Schell, J.A., Deering, D.W., 1973. Monitoring the vernal advancement and retrogradation (green wave effect) of natural vegetation. Prog. Rep. RSC https://ntrs.nasa.gov/citations/19730009608 (1978-1).
Roy, D.P., Li, Z., Zhang, H.K., Huang, H., 2020. A conterminous United States analysis of the impact of Landsat 5 orbit drift on the temporal consistency of Landsat 5 Thematic Mapper data. Remote Sens. Environ. 240. https://doi.org/10.1016/j.rse.2020.111701.
Stull, R.B., 1988. An Introduction to Boundary Layer Meteorology.
Suárez, F., Lobos, F., de la Fuente, A., de Arellano, J.V.G., Prieto, A., Meruane, C., Hartogensis, O., 2020. E-DATA: a comprehensive field campaign to investigate evaporation enhanced by advection in the hyper-arid altiplano. Water (Switzerland) 12. https://doi.org/10.3390/w12030745.
Tejeda, I., Cienfuegos, R., Munoz, J.F., Durán, M., 2003. Numerical modeling of saline intrusion in Salar de Atacama. J. Hydrol. Eng. 8. https://doi.org/10.1061/(ASCE)1084-0699(2003)8:1(25).
Tölgyesi, C., Zalatnai, M., Erdos, L., Bátori, Z., Hupp, N.R., Körmöczi, L., 2015. Unexpected ecotone dynamics of a sand dune vegetation complex following water table decline. J. Plant Ecol. 9. https://doi.org/10.1093/jpe/rtv032.
Tulbure, M.G., Broich, M., 2013. Spatiotemporal dynamic of surface water bodies using Landsat time-series data from 1999 to 2011. ISPRS J. Photogramm. Remote Sens. https://doi.org/10.1016/j.isprsjprs.2013.01.010.
Uribe, J., Muñoz, J.F., Gironás, J., Oyarzún, R., Aguirre, E., Aravena, R., 2015. Assessing groundwater recharge in an Andean closed basin using isotopic characterization and a rainfall-runoff model: Salar del Huasco basin, Chile. Hydrogeol. J. 23, 1535–1551. https://doi.org/10.1007/s10040-015-1300-z.
Vásquez, C., Ortiz, C., Suárez, F., Muñoz, J.F., 2013. Modeling flow and reactive transport to explain mineral zoning in the Atacama salt flat aquifer, Chile. J. Hydrol. 490. https://doi.org/10.1016/j.jhydrol.2013.03.028.
Wetzel, R.G., 2001. Limnology: Lake and River Ecosystems. Academic Press.
Wilkinson, G.M., Walter, J., Fleck, R., Pace, M.L., 2020. Beyond the trends: the need to understand multiannual dynamics in aquatic ecosystems. Limnol. Oceanogr. Lett. https://doi.org/10.1002/lol2.10153.
Yechieli, Y., Wood, W.W., 2002. Hydrogeologic processes in saline systems: playas, sabkhas, and saline lakes. Earth Sci. Rev. 58. https://doi.org/10.1016/S0012-8252(02)00067-3.